2021 43rd Annual International Conference of the
IEEE Engineering in Medicine & Biology Society (EMBC)
Oct 31 - Nov 4, 2021. Virtual Conference

A System for Co-Registration of High-Resolution Ultrasound, Magnetic Resonance Imaging, and Whole-Mount Pathology for Prostate Cancer

Jake Pensa, Wayne Brisbane, Alan Priester, Anthony Sisk, Leonard Marks, Rory Geoghegan, *Member, IEEE*

***Abstract*— In order to evaluate the diagnostic accuracy of high-resolution ultrasound (HRUS) for detection of prostate cancer, it must be validated against whole-mount pathology. An ex-vivo HRUS scanning system was developed and tested in phantom and human tissue experiments to allow for in-plane computational co-registration of HRUS with magnetic resonance imaging (MRI) and whole-mount pathology. The system allowed for co-registration with an error of 1.9mm±1.4mm, while also demonstrating an ability to allow for lesion identification.**

***Clinical Relevance*— Using this system, a workflow can be established to co-register HRUS with MRI and pathology to allow for the diagnostic accuracy of HRUS to be determined with direct comparison to MRI.**

I. Introduction

Prostate Cancer is the most common internal malignancy and second leading cause of cancer death in men, with approximately 250,000 new cases and 34,000 deaths expected in 2021 [1], [2]. Ultrasound (US) guided biopsy is a common approach for diagnosing prostate cancer [3]. Conventional US (2-15MHz) frequently fails to detect prostate cancer, with retrospective studies showing that up to 40% of tumors are isoechoic under US and indistinguishable from surrounding tissue [4]–[6]. Magnetic resonance imaging (MRI) has a higher detection rate, but still misses 15-20% of clinically significant prostate cancer and underestimates tumor volumes by as much as 300% [7]–[9]. Thus, the current recommended diagnostic strategy is either an MRI guided biopsy or an MR-US fusion biopsy [10]. For fusion biopsies, a previous MRI scan with a segmented suspicious lesion is fused to an US scan in real time allowing for MRI lesions to be visualized under US for quick and accurate biopsies [11]. As a diagnostic tool, MRI is resource intensive, has large interobserver variability, and requires an additional procedure for the patient [12]. These drawbacks currently limit MRI targeted biopsies to large academic centers.

Recently, high-resolution ultrasound (HRUS), also known as micro-ultrasound, has been introduced for prostate cancer diagnosis. Commercially available machines operate at a much higher frequency (29MHz) than conventional US probes, while maintaining an imaging depth of 6cm, allowing for a superior spatial resolution of approximately 70µm versus 200µm for conventional ultrasound [13]. The matching of HRUS readings to 400 tracked biopsies led to the development of the Prostate Risk Identification using Micro-Ultrasound (PRI-MUS) grading scale for detecting and grading prostate cancer [14]. In preliminary studies HRUS has performed similarly to MRI and could potentially provide a low cost alternative to MRI for targeted biopsies [13].

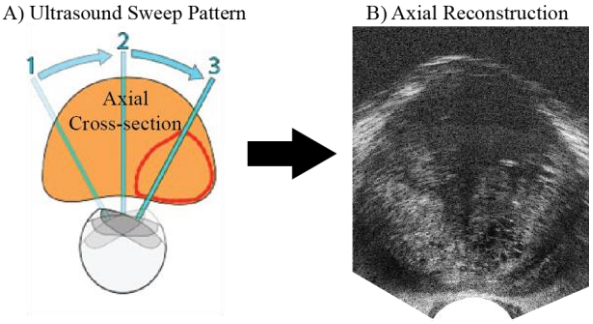

Figure 1. A) HRUS imaging is achieved by sweeping the imaging plane across the prostate. B) Axial reconstruction degrades image quality, particularly in areas distant from the US probe, thus, preventing accurate registration with WM pathology.

HRUS has demonstrated potential for prostate cancer diagnosis, however, it lacks validation to whole-mount (WM) pathology, the gold standard. WM pathology is a clinical practice to serially section an entire prostate gland, while preserving three-dimensional orientation to allow for anatomical localization of tumor margins [15]. Some hospitals create custom 3D printed molds for each patient to ensure sectioning in the axial orientation [7]. HRUS utilizes a side fire probe, therefore, in-vivo imaging is achieved by sweeping the ultrasound plane across the prostate in a fan shaped pattern (Fig 1a). Since WM pathology is acquired in the axial orientation, computational registration is challenging even with highly-controlled scanning setups (Fig 1b) [16]. Here we present a scanning system that facilitates accurate in-plane co-registration of ex-vivo HRUS with WM pathology and MRI for eventual comparison of the diagnostic accuracy of both imaging modalities against WM pathology.

II. Methods

A. Ex-Vivo Scanning System Design

In order to perform an ex-vivo scan of a human prostate, a custom HRUS scanning system was designed and manufactured as shown in Fig. 2a. It consists of a HRUS probe

*Research supported by Exact Imaging™.

J. Pensa, W. Brisbane, A.Priester, A. Sisk, L. Marks, and R. Geoghegan, are with the Department of Urology, University of California, Los Angeles, CA 90025, USA. (email: jake.pensa@gmail.com)

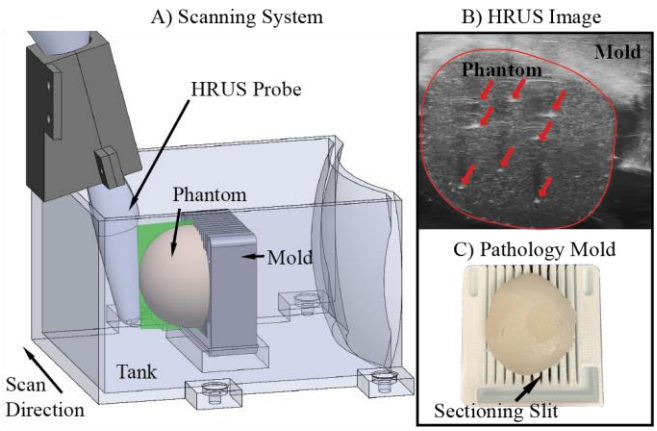

Figure 2. Ex-vivo scanning gantry used to scan phantoms and prostates secured in 3D printed molds. The prostate is scanned in the axial orientation from apex to base in 70µm increments. The US image plane is represented in green. The fiducial needle tracks are marked in the HRUS image with red arrows. The histology slides are prepared by sectioning through the slits in the pathology mold.

(ExactVu, Exact Imaging. Ontario) mounted to an electronic translation stage (X-USBDC, Zaber Technologies Inc. British Columbia) via a custom 3D printed attachment. The imaging tank was 3D printed (Lulzbot Taz 6, Fargo Additive Manufacturing Equipment 3D LLC. USA) in polylactic acid (PLA) and water sealed with silicon sealant spray. The imaging tank was designed to allow for one half of a pathology mold to be secured inside. In our institution, these 3D printed pathology molds are routinely used to ensure axial sectioning during preparation of histology slides. This enables both cognitive and computational co-registration to axial MRI [17]. The imaging specimen is placed inside the anterior portion of the pathology mold, which is in turn placed in the imaging tank in an orientation to allow for axial HRUS images to be acquired as the probe translates laterally from the apex to the base across the specimen. The probe was translated at a speed of 0.65mm/sec to allow for images to be taken approximately every 70µm given the probe has an image capture rate of 9 fps. This provides a densely sampled image set of the specimen that allows for later reconstruction.

To further improve the HRUS scan quality, two different types of pathology molds were tested. One mold was a traditional pathology slicing mold made of PLA and the other was made of Thermoplastic polyurethane (TPU). An agar phantom (4%w/v) was scanned in the HRUS scanning gantry using both molds. The subsequent image stacks were compared qualitatively and quantitatively to assess the impact of the material properties on the imaging artifacts, full width at half maximum (FWHM) at the edge of the mold, pixel intensities, signal to noise ratios (SNR), and contrast to noise ratios (CNR). A superior mold generates less noise and has sharper edges, generally characterized by a short FWHM, high SNR and CNR, and low background pixel intensities.

B. *Process for Co-Registration of Ex-Vivo Scans with Whole-Mount Pathology*

A custom MATLAB script was developed to co-register images acquired by the scanning gantry to axial histology slices. The software was validated in 5 unique agar phantoms (4%w/v) as described in a prior study [17]. Briefly, warm agar solution was poured into a prostate mold with needles oriented in specific positions throughout the prostate and then placed in a refrigerator to cool. Once the agar set, the needles were removed leaving behind tracks that serve as fiducial markers. The prostate phantoms were then removed and placed in custom pathology molds and scanned in the gantry with the HRUS probe (Fig. 2b). The phantoms were subsequently sliced axially in the full pathology mold (Fig. 2c) and scanned on a conventional desktop scanner (MFC-9340CDW, Brother Industries, Ltd. Japan) at 600dpi to mimic WM pathology slides. Using a DICOM viewer (Horos, Horos Project), both the HRUS and desktop scan of the phantom were segmented and the fiducials were marked. With the prostate capsule as the basis for co-registration, the segmentations were then co-registered via a custom MATLAB script. This was performed through a rigid transformation of the sliced phantoms to account for scaling and in-plane rotational misalignment, followed by a non-rigid thin-plate spline transformation using control points on the prostate capsule to account for non-rigid specimen deformation as described by Fei et al. [18]. The in-plane distance between matched fiducials on HRUS and desktop scans was recorded for each fiducial pair and used for determining in-plane target registration error (TRE).

C. *Pilot Clinical Study*

After adequate in-plane co-registration and image quality had been achieved, the ex-vivo scanning gantry was validated in a clinical trial. All research involving human subjects was approved by the Institutional Review Board. Three patients set to undergo radical prostatectomy were consented and enrolled in the study. Using a pre-operative MRI scan with annotated suspicious lesions, custom PLA and TPU molds were printed for prostate slicing and imaging respectively. Following radical prostatectomy and prior to fixation, the prostate was placed in the anterior half of a TPU mold, secured via a suture, and imaged with HRUS in the ex-vivo scanning gantry in the same manner as the phantom scans. After scanning, the prostate was placed in the PLA pathology mold and sectioned axially following routine clinical protocol. Histology slides were made from each slice and cancerous lesions were annotated by an experienced pathologist. The annotated slides were subsequently scanned at high resolution (20x). Following a similar process to the phantom experiment, the histology slides were then cognitively compared to the HRUS scan and pre-operative MRI to find matched image triplicates. The prostate and visible lesions were identified and segmented by separate expert blinded observers for the HRUS scan, MRI scan, and pathology slides. Following metrics used in similar studies [19], [20], the overlap percentage, DICE similarity coefficient (DSC), and centroid distance were calculated for each co-registered region of interest (ROI) triplicate. This allows for preliminary analysis of the ability of HRUS to identify lesions, using MRI imaging as a benchmark.

III. Results

A. *Ex-Vivo Scanning System Design*

A total of 477 matched images were compared between a phantom imaged in both PLA and TPU molds (Fig 3). Matched background pixels (N = 96,000) were compared between PLA and TPU with the former exhibiting a higher average pixel intensity by 27.5±54.8. From a sample of 50 images for each mold, the FWHM was found to be 4.6mm±1.1mm for PLA and 1.8mm±0.4mm for TPU,

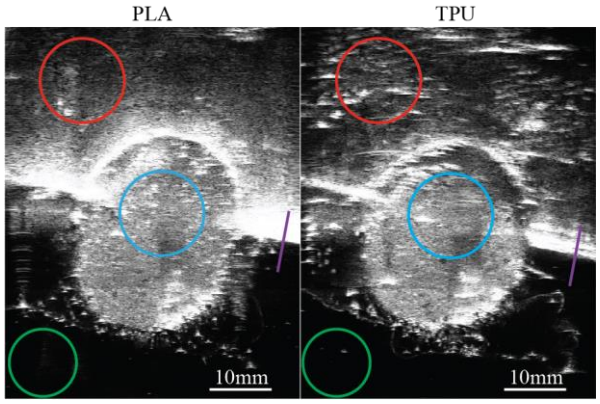

Figure 3. Comparison of PLA and TPU phantom images. (Red) Background noise within the mold. (Blue) Signal from the phantom. (Green) Background noise in the water. (Purple) FWHM across the interface between the mold and the water.

indicating the TPU molds have sharper edges under HRUS. For a sample of 100 images, the SNR was found to be 84.2 and 97.8 for PLA and TPU respectively. The CNR for PLA was 43.3 and 72.5 for TPU. These data indicate that TPU molds result in fewer imaging artifacts, sharper edges, better signal and contrast to noise ratios. Due to the superior imaging quality, the TPU mold was chosen for imaging ex-vivo human prostates as outlined in the next section.

B. Process for Co-Registration of Ex-Vivo Scans with Whole-Mount Pathology

From the 5 agar phantoms, a total of 294 matched fiducial pairs were compared from 40 phantom slices (Fig 4). The average in-plane TRE was 1.9mm±1.4mm. This is similar to the TRE observed when co-registering axial MRI to WM pathology (1.9mm±0.6mm) [17].

C. Pilot Clinical Study

From 3 subjects, a total of 14 HRUS, MRI and pathology image triplicates were matched and computationally registered together (Fig 5). Lesions were present on 11 of the pathology slides with a total of 20 distinct lesions. Of these 20 lesions 13 were identified by the HRUS observer with only 4 identified on MRI. Overall, 26 lesions were delineated on HRUS with 18 true positives and 8 false positives. For MRI,

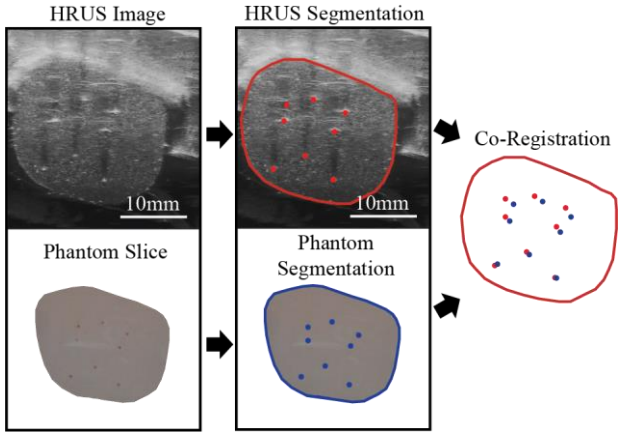

Figure 2. Co-Registration of HRUS images with phantom slices. The phantom capsule and needle track fiducials were marked on both and co-registered using a custom MATLAB script.

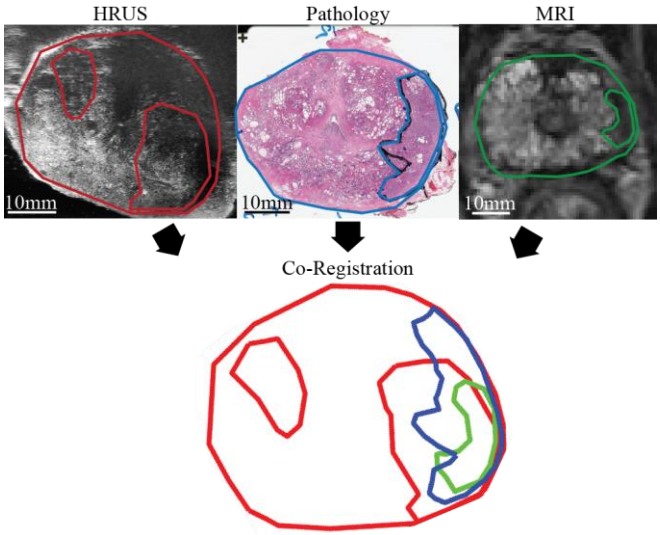

Figure 5. Co-Registration of HRUS (red) and MRI (green) images with WM pathology (blue) slides. The capsules and lesions are marked on each modality.

4 true positive lesions were delineated. The average distance between the centroids of the true positive HRUS ROIs and the actual lesions was 10.8mm±7.2mm with 11 out of 26 of the ROIs having a centroid distance from the WM ROI of less than 1cm. For MRI the average centroid distance was 5.8mm±2.5mm with all 4 ROIs having a centroid distance of less than 1cm from the WM ROI. The average overlap percentage and average DSC of the true positive HRUS and WM ROIs was 54.3%±33.1% and 0.33±0.21 respectively. While for MRI the average overlap percentage was 85.1%±17.6% and DSC was 0.61±0.05.

IV. Discussion

The goal of this study was to develop and validate an ex-vivo scanning system to allow for in-plane co-registration of HRUS and MRI images with WM pathology, for eventual comparison of the diagnostic accuracy of HRUS versus MRI imaging. Phantom experiments demonstrated that the developed scanning gantry facilitates in-plane co-registration similar to published values for MRI with a TRE of 1.9mm±1.4mm [17]. This error is considered acceptable given that the average biopsy needle deflection is 0.9mm and the average registration error for MR-US fused biopsies is 1.2mm±1.1mm [21], [22]. However, the phantoms are more rigid than prostate tissue, so there may be a larger TRE than was found with the phantoms from increased deformation when sectioning. This study also found TPU molds offer superior imaging quality to PLA. This is likely due to the reduced material stiffness of TPU resulting in a lower acoustic impedance difference at both the water-mold interface and the phantom-mold interface.

Overall, the ex-vivo scanning system allowed for detection of prostate cancer with 65% of distinct lesions and all 3 index lesions correctly identified under HRUS. The index lesion is the largest and most aggressive tumor and believed to be responsible for the progression of prostate cancer making its detection vital for proper disease management [23], [24]. Additionally, 6 out of the 7 lesions that HRUS failed to detect, were small lesions with a cross-sectional area less than 40mm^2. The only large lesion that was missed by HRUS was located

in the far anterior of the prostate, indicative of a weakness of HRUS as there is a distinct loss of resolution in the far anterior of the prostate due to shadowing, however this lesion was also missed under MRI. This lack of imaging resolution at depth does not have much clinical relevance as analysis from the UCLA database of 1348 biopsy-confirmed MRI visible tumors shows that 93.8% of prostate cancer has been reported to be located within 3cm of the posterior capsule of the prostate [25].

The pilot clinical study demonstrated the scanning system and registration software presented here are capable of co-registering ex-vivo HRUS with MRI and WM pathology. Ultimately, this facilitated comparison of the clinical utility of HRUS and MRI using WM pathology as ground truth. However, it should be noted that HRUS scans were performed ex-vivo and is not indicative of a clinical scan, while MRI was performed in-vivo. In an in-vivo setting there are anatomical structures which can potentially degrade image quality, but ex-vivo also has structures that could also degrade image quality such as the TPU mold and tank. Further analysis is planned to evaluate the differences between ex-vivo and in-vivo imaging.

The clinical data present here highlight the promise of HRUS as an alternative to MRI for prostate cancer detection as all 3 index lesions were correctly identified. However, this was only an exploratory study with a small sample size (N=3), therefore, accurate metrics for the sensitivity and specificity of HRUS cannot be discerned. Further work is planned to increase the number of patients and ultimately demonstrate the clinical utility of HRUS.

V. Conclusion

The scanning system presented here facilitated accurate in-plane co-registration of ex-vivo HRUS and MRI images with WM pathology slides. As demonstrated in the pilot clinical study, this process enables rigorous assessment of the utility of HRUS for prostate cancer detection. Further work is planned in which the scanning system will be used in a larger clinical trial to determine the sensitivity and specificity of HRUS.

Acknowledgment

The authors would like thank Dr. Brian Wodlinger PhD with Exact Imaging^{TM} for his assistance with this project.

References

[1] M. R. Cooperberg and P. R. Carroll, "Trends in management for patients with localized prostate cancer, 1990-2013," *JAMA - J. Am. Med. Assoc.*, vol. 314, no. 1, pp. 80–82, Jul. 2015.

[2] R. L. Siegel, K. D. Miller, H. E. Fuchs, and A. Jemal, "Cancer Statistics, 2021," *CA. Cancer J. Clin.*, vol. 71, no. 1, pp. 7–33, Jan. 2021.

[3] M. E. Noureldin, M. J. Connor, N. Boxall, S. Miah, T. Shah, and J. Walz, "Current techniques of prostate biopsy: An update from past to present," *Translational Andrology and Urology*, vol. 9, no. 3. AME Publishing Company, pp. 1510–1517, 01-Jun-2020.

[4] K. Shinohara, T. M. Wheeler, and P. T. Scardino, "The appearance of prostate cancer on transrectal ultrasonography: Correlation of imagining and pathological examinations," *J. Urol.*, vol. 142, no. 1, pp. 76–82, 1989.

[5] F. A. Ganie *et al.*, "Correlation of transrectal ultrasonographic findings with histo pathology in prostatic cancer.," *J. Educ. Health Promot.*, vol. 3, no. 1, pp. 38–38, 2014.

[6] K. K. Shung, "High Frequency Ultrasonic Imaging," *Journal of Medical Ultrasound*, vol. 17, no. 1. Elsevier (Singapore) Pte Ltd, pp. 25–30, 2009.

[7] A. Priester *et al.*, "Magnetic Resonance Imaging Underestimation of Prostate Cancer Geometry: Use of Patient Specific Molds to Correlate Images with Whole Mount Pathology," *J. Urol.*, vol. 197, no. 2, pp. 320–326, Feb. 2017.

[8] H. U. Ahmed *et al.*, "Diagnostic accuracy of multi-parametric MRI and TRUS biopsy in prostate cancer (PROMIS): a paired validating confirmatory study," *Lancet*, vol. 389, no. 10071, pp. 815–822, Feb. 2017.

[9] D. C. Johnson *et al.*, "Detection of Individual Prostate Cancer Foci via Multiparametric Magnetic Resonance Imaging," *Eur. Urol.*, vol. 75, no. 5, pp. 712–720, May 2019.

[10] M. A. Bjurlin *et al.*, "Update of the Standard Operating Procedure on the Use of Multiparametric Magnetic Resonance Imaging for the Diagnosis, Staging and Management of Prostate Cancer," *J. Urol.*, vol. 203, no. 4, pp. 706–712, Apr. 2020.

[11] L. Marks, S. Young, and S. Natarajan, "MRI-ultrasound fusion for guidance of targeted prostate biopsy.," *Curr. Opin. Urol.*, vol. 23, no. 1, pp. 43–50, Jan. 2013.

[12] A. B. Rosenkrantz *et al.*, "Interobserver reproducibility of the PI-RADS version 2 lexicon: A multicenter study of six experienced prostate radiologists," *Radiology*, vol. 280, no. 3, pp. 793–804, Sep. 2016.

[13] L. Klotz *et al.*, "Comparison of micro-ultrasound and multiparametric magnetic resonance imaging for prostate cancer: A multicenter, prospective analysis," *Can. Urol. Assoc. J.*, vol. 15, no. 1, p. E11, Jul. 2020.

[14] S. Ghai *et al.*, "Assessing Cancer Risk on Novel 29 MHz Micro-Ultrasound Images of the Prostate: Creation of the Micro-Ultrasound Protocol for Prostate Risk Identification," *J. Urol.*, vol. 196, no. 2, pp. 562–569, Aug. 2016.

[15] N. J. Look Hong, G. M. Clarke, M. J. Yaffe, and C. M. B. Holloway, "Cost-effectiveness analysis of whole-mount pathology processing for patients with early breast cancer undergoing breast conservation," *Curr. Oncol.*, vol. 23, no. Suppl 1, pp. S23–S31, 2016.

[16] M. L. Palmeri *et al.*, "Identifying Clinically Significant Prostate Cancers using 3-D In Vivo Acoustic Radiation Force Impulse Imaging with Whole-Mount Histology Validation," *Ultrasound Med. Biol.*, vol. 42, no. 6, pp. 1251–1262, Jun. 2016.

[17] A. Priester *et al.*, "Registration Accuracy of Patient-Specific, Three-Dimensional-Printed Prostate Molds for Correlating Pathology with Magnetic Resonance Imaging," *IEEE Trans. Biomed. Eng.*, vol. 66, no. 1, pp. 14–22, Jan. 2019.

[18] B. Fei, C. Kemper, and D. L. Wilson, "A comparative study of warping and rigid body registration for the prostate and pelvic MR volumes," *Comput. Med. Imaging Graph.*, vol. 27, no. 4, pp. 267–281, Jul. 2003.

[19] K. H. Zou *et al.*, "Statistical Validation of Image Segmentation Quality Based on a Spatial Overlap Index," *Acad. Radiol.*, vol. 11, no. 2, pp. 178–189, 2004.

[20] M. Piert *et al.*, "Accuracy of tumor segmentation from multi-parametric prostate MRI and 18F-choline PET/CT for focal prostate cancer therapy applications," *EJNMMI Res.*, vol. 8, no. 1, p. 23, Dec. 2018.

[21] S. Natarajan *et al.*, "Clinical application of a 3D ultrasound-guided prostate biopsy system," *Urologic Oncology: Seminars and Original Investigations*, vol. 29, no. 3. Urol Oncol, pp. 334–342, May-2011.

[22] N. N. Stone *et al.*, "Deflection Analysis of Different Needle Designs for Prostate Biopsy and Focal Therapy," *Technol. Cancer Res. Treat.*, vol. 16, no. 5, pp. 654–661, Oct. 2017.

[23] A. Stabile, M. Moschini, F. Montorsi, X. Cathelineau, and R. Sanchez-Salas, "Focal therapy for prostate cancer-index lesion treatment vs. hemiablation. A matter of definition," *International Braz J Urol*, vol. 45, no. 5. Brazilian Society of Urology, pp. 873–876, 2019.

[24] H. U. Ahmed, "The Index Lesion and the Origin of Prostate Cancer," *N. Engl. J. Med.*, vol. 361, no. 17, pp. 1704–1706, Oct. 2009.

[25] W. Brisbane and L. Marks, "Analysis of UCLA Prostate Biopsy Database." unpublished.